processes

MDPI

Article

A Novel Back-Stepping Sliding Mode Control Strategy of Direct-Drive Wave Energy Converters

Shiguang Weng and Jianyong Wang *

Institute of Marine, Xiamen Ocean Vocational College, Xiamen 361012, China; xmocwsg@163.com
* Correspondence: meiminwang@163.com; Tel.: +86-0592-5393-525

Abstract: In this paper, a maximum energy extraction and tracking strategy for direct-drive wave energy converters (DDWECs) based on back-stepping and sliding mode control strategies are developed. It is well known that the existence of the chattering phenomenon degrades the control performance of conventional sliding mode control (SMC). To mitigate the effects of flutter and external disturbances, a back-stepping sliding model control (BSMC) scheme is proposed. The main features of the proposed methodology are as follows: (1) By using the proposed BSMC, the maximum wave energy of DDWEC can be captured. Moreover, the speed tracking of the permanent magnet linear generator (PMLG), which is a subsystem of DDWEC, tracked in real-time. (2) By virtue of the proposed BSMC, the closed-loop control system is asymptotically stable in finite time. (3) With the superior controllability of the BSMC, it can handle disturbances that the SMC cannot handle. Comprehensive and comparative studies are proved to be superior to the most advanced method

Keywords: direct-drive wave energy converters; permanent magnet linear generator; wave energy tracking; back-stepping sliding mode control

Citation: Weng, S.; Wang, J. A Novel Back-Stepping Sliding Mode Control Strategy of Direct-Drive Wave Energy Converters. *Processes* **2022**, *10*, 1385. https://doi.org/10.3390/pr10071385

Academic Editors: Eugen Rusu, Kostas Belibassakis, George Lavidas and Ján Piteľ

Received: 7 June 2022
Accepted: 13 July 2022
Published: 15 July 2022

1. Introduction

The ocean is rich in fossil energy, biological resources, and renewable energy. As a representative of marine renewable energy, wave energy can persistently preserve large power density [1]. Wave energy generation has become a hot topic in both academia and industry. Due to the harsh environments under which marine power generation systems work, the development of wave energy generation is very challenging. With incremental advances and efforts, emerging wave energy power plants are launching for commercial operations [2]. Accordingly, it is extremely urgent to develop reliable, high-performance wave energy generation systems.

It is well known that the power capture and energy conversion modules play key roles in wave energy generation systems. Mechanical structure, hydrodynamic aspect, and energy conversion rate of various WECs are the questions that researchers pay more attention to [3]. There are many challenges, such as the complexity of hydrodynamic system design, power take-off efficiency, and effectiveness of the designed control methods, which hinder the development of this technology [4]. A reactive control method is proposed to achieve optimal control by expanding the effective bandwidth of the power generation equipment [5]. A latching control approach is proposed in [6], which uses the float speed to match the frequency of WECs. In [7], hydrodynamic equation of Archimedes wave swing (AWS) was established. Dynamic models of the AWS were simulated by RLC circuits, whereby the single-double degree of freedom method was proposed to construct optimal power transmission conditions. However, control issues of the generator were not addressed. In the past ten years, researchers attempted to use physical methods to change the natural frequency of wave energy generators. Shek et al. [8] developed adjustable energy conversion devices to control the velocity of linear generators such that motion amplitude and phase of wave energy converters (WECs) can be regulated. However, reactive power

was inevitably generated during system operation, thereby causing additional losses. In [9], Bacelli analyzed the optimal wave energy acquisition conditions under passive damping control and proposed a control method of conditional damping to deal with the limitations of wave energy power generation devices. In [10], Marei draws on the tracking control methods of wind energy and solar energy, and proposes an optimal power point tracking method on the PTO side, and adjusts parameters according to the disturbance observation method to achieve maximum wave energy capture. In [11] proposed a phase control method for tracking the displacement of waves for direct-drive wave energy generation systems, which directly controls the counter electromagnetic force to achieve resonance between the wave energy generation device and the wave and improves the working efficiency of the wave energy generation system. In [12], Mehdi Neshat conducts a comprehensive investigation, evaluation, and comparison of the optimization of the geometry, tether angles, and power take-off (PTO) settings of a wave energy converter (WEC) using bio-inspired swarm-evolutionary optimization algorithms.

With the extensive research on wave energy converters, the most recent objective of the research on wave energy converters is the development of an integrated analysis of power transformation from sea waves to the electric wire, it would highlight the importance of energy maximization during the whole operation of the systems and of the control strategies. Oscillating water column (OWC) devices can greatly improve the energy conversion efficiency of wave energy. In [13], an application of an analytical wave-to-wire model of an OWC device for the preliminary optimization of these systems for a small installation in a moderate wave climate in the Mediterranean Sea, is presented, which determines power transformation from sea waves to the electric wire through a fast and reliable approach. In [14], a wave-to-wire model for OWC systems based on an impulse air turbine is provided. The model performs a comprehensive simulation of the system to estimate the attendant electric energy production for a specific sea state, based on analytical models of the primary (fixed chamber) and secondary (air turbine) converters coupled with the tertiary converter (electric generator). In [15], a detailed analysis of the dynamics and control of air turbines and electrical generators in OWCs) is presented. The aim is to provide a detailed generator model based on experimental data to assess the influence of the generator efficiency on the power take-off performance. Another important conclusion is that the selection of the control law is tightly related to the efficiency of the selected generator. The generator should have the maximum efficiency along the operating path of the control law that maximizes the turbine power output. A critical characteristic of most WECs is the large peak-to-average power ratio; the greatest advantage of OWC-based WECs is the ability to control or dissipate any excess of energy available to the PTO system that may occur in medium to highly energetic sea states. In [16], a performance assessment of a new control algorithm to operate an HSSV (high-speed stop valve) installed in series with the turbine. The proposed control algorithm shows large improvements in the extracted mean power while limiting the peak-to-average power ratio, thus improving the power quality delivered to the electrical grid.

In terms of energy conversion, maximum power point tracking (MPPT) is widely pursued in renewable energy industries. Most of them were used in solar power generation [17–20]. Based on the previous literature, the MPPT heuristic-based techniques, such as PSO and GWO, suffer from oscillations around the global maximum power point (GMPP); in addition, they cannot catch the variant GMPP under variant PSC. To deal with this problem, GWO is hybridized with fuzzy logic controller (FLC) controller to reduce the oscillations in power around the GMPP is proposed in [17]. In [18], a new mitigating solution for interharmonics in PV systems is proposed. The proposed method modifies the MPPT algorithm in a way to randomly select the sampling rate between the fast and the slow value. By doing so, the interharmonics in the output current can be effectively reduced due to the distribution of the frequency spectrum. In [19], a novel MPPT method based on a voltage reference estimator (VRE) combined with a fuzzy logic controller (FLC) is proposed to obtain the maximum power from the PV panel. In [20], an efficient and

robust MPPT controller using novel Slime mold optimization (SMO) and improved salp swarm optimization algorithm (ISSA) is proposed to track GMPP for different PV array configurations. In [21,22], the MPPT technology has been applied to wind power generation. In [21], a current decoupling controller for a Doubly-fed Induction Generator (DFIG) based on a floating offshore wind turbine and power to gas is proposed, which realizes Maximum Power Point Tracking (MPPT) through integral sliding mode compensation. By using the internal model control strategy, an open-loop controller is designed to ensure that the system has good dynamic performance. In [22], three new maximum power point tracking control schemes are proposed for permanent magnet synchronous generators in variable-speed wind energy conversion systems. Unlike previously control methods based on traditional voltage source fed equivalent circuit, a current source fed equivalent circuit is proposed where an efficient maximum power point tracking–based load angle control can simply be achieved.

Note that the wave power generation system involves strong nonlinearities and couplings. In this context, the MPPT objective pertaining to wave energy generation becomes much more challenging. In [23], an MPPT strategy has been proposed to maximize wave energy conversion in real-world wave environments. In [24], a nonlinear internal model control (IMC) method was developed by virtue of system estimation. It should be noted that uncertainties cannot be sufficiently suppressed. In [25], the fuzzy control approach was incorporated into the MPPT framework, whereby historical data of amplitude of wave incidence and average power captured by systems were exploited and the genetic algorithm was used to estimate system dampings. However, the foregoing method only considered wave amplitude and average power captured by the conversion system as optimization parameters. Inspired by the MPPT method in [26], a variable characteristic curve control scheme has been developed for wind power generation systems [27]. It has been verified by experiments that power generation can be enhanced since the electromagnetic torque fluctuation can be avoided.

Recently, model predictive control (MPC) has become an attractive candidate for WEC systems because of its ability to generate high-performance tracking in the presence of unspecific modeled dynamics [28,29]. In [28], a novel feedback noncausal model predictive control (MPC) strategy for sea wave energy converters(WECs) is proposed, where the wave prediction information can be explicitly incorporated into the MPC strategy to improve the WEC control performance. In [29], an economic feedback model predictive control scheme is proposed to improve the energy conversion efficiency of wave energy converters (WECs) and guarantee their safe operation over a wide range of sea conditions. In [30], a nonlinear model predictive control strategy is proposed and applied to model-scale point absorbers to maximize their power absorption in regular and irregular sea conditions. However, it is difficult to identify the system model online. In [31], both reactive and latching control strategies were proposed. The proposed control strategies have improved the peak-to-average power ratios. Unfortunately, the system's mechanical and maintenance costs were increased.

In this paper, a new phase control method is proposed, which does not need the mechanical structure of active phase control and can absorb the maximum power. The main contributions of this paper are as follows:

1. The entire direct-drive wave energy conversion (DDWEC) system is divided into main and control circuits, whereby the former consists of the float, permanent magnet linear generator (PMLG), rectifier, and load. In this work, we focus on the velocity control of DDWEC, which can be affected by the anti-electromagnetic force of PMLG. By employing a series of axis transformations, the PMLG current signal is changed from the abc frame of reference to the dq frame of reference.
2. To facilitate the design of the motor controller, a zero d-axis vector control scheme is selected. Next, a BSMC scheme is designed to use the actual current and reference current of the d-axis and q-axis as inputs of the controller.

3. To accurately and quickly track d-axis and q-axis current signals, control voltage signals of the SVPWM pulse generator are generated. The rectifier circuit is driven by the pulse to work. PMLG's anti-electromagnetic is affected by the load characteristics of the main circuit, whereby the velocity of PMLG is affected. Eventually, the velocity of PMLG is in phase with the incident wave force. The entire system resonance is reached. The incident wave energy of DDWEC is adsorbed to the utmost.

The organization of the paper is as follows. In Section 2, the WEC is formulated with necessary preliminaries. The proposed BSMC scheme, together with stability analysis, is presented in Section 3. Section 4 presents simulation results that demonstrate the effectiveness and efficiency of the proposed control strategy. Finally, conclusions are drawn in Section 5.

2. PMLG Dynamic Modeling

The structure diagram of the DDWEC device is shown in Figure 1. A key feature of direct-drive wave energy conversion systems is the use of linear motors as generators compared to wave energy conversion using hydraulic or pneumatic systems. The PMLG is driven to convert the mechanical energy captured by the wave energy capture device into electrical energy. Line generator is directly used in the direct-drive wave energy system, and the energy conversion loss of wave is reduced at the same time.

The flowchart is shown in Figure 2. Under the action of the wave, the converter of the linear generator oscillates vertically, and the wind passes through the magnetic field line, producing the induced voltage and electric power. Subsequently, the production of electricity is connected to electrical equipment and batteries through a power electronic converter.

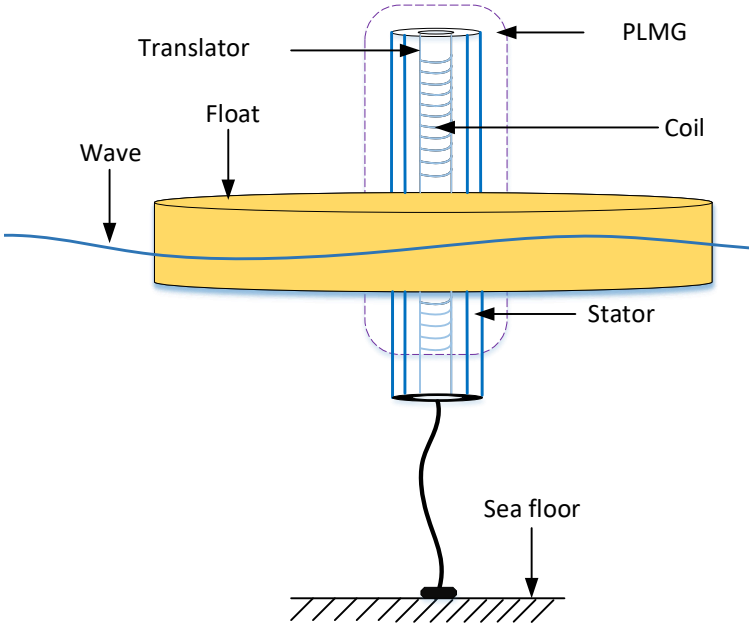

Figure 1. Direct-drive wave energy conversion device structure.

Considering the wave force in the vertical direction of the buoy, the wave energy conversion device is equivalent to a vibration structure composed of a spring and a mass. The DDWEC dynamics are governed by

$$m\ddot{x} = f_e + f_r + f_b + f_v + f_f + f_g - mg \tag{1}$$

where m is the mass of the wave energy conversion system, x is the vertical position of the PMLG rotor, f_e is wave excitation force, f_r is radiation force, f_b is the static buoyancy of the

buoy in water, f_v is the viscous force, f_f is friction force, and f_g is the anti-electromagnetic force of PMLG. Here,

$$f_r = -m_a(\omega)\ddot{x}(t) - \int_{-\infty}^{t} R_a(\tau)\dot{x}(t-\tau)\mathrm{d}\tau \quad (2)$$

$$f_b = -kx + mg \quad (3)$$
$$= -\rho g S x + mg$$

$$f_g = -R_g\dot{x} - k_g x \quad (4)$$

$$f_e = k_{ex}(t) * \eta \quad (5)$$

where m_a is the additional quality of the system, R_a is the additional damping of the system, R_g is the damping coefficient of the linear generator's active power capability, k represents the buoyancy factor, ρ is the water density and S is the area where the buoy contact with wave, g is the acceleration of gravity, k_g is the elastic coefficient of the linear generator's absorption of reactive power, $k_{ex}(t)$ is the excitation convolution kernel and η is the measured wave elevation.

Ignoring viscous force and friction force, (1) can be simplified to

$$(m + m_a)\ddot{x} + (R_a + R_g)\dot{x} + (k + k_g)x = f_e \quad (6)$$

The simplified model of DDWEC dynamics can be rewritten as follows:

$$M\ddot{x} = f_e - R_a\dot{x} - kx + f_g \quad (7)$$

$$f_g = -R_g\dot{x} - k_g x \quad (8)$$

where M is the total mass of the DDWEC and f_g is the anti-electromagnetic force of PMLG.

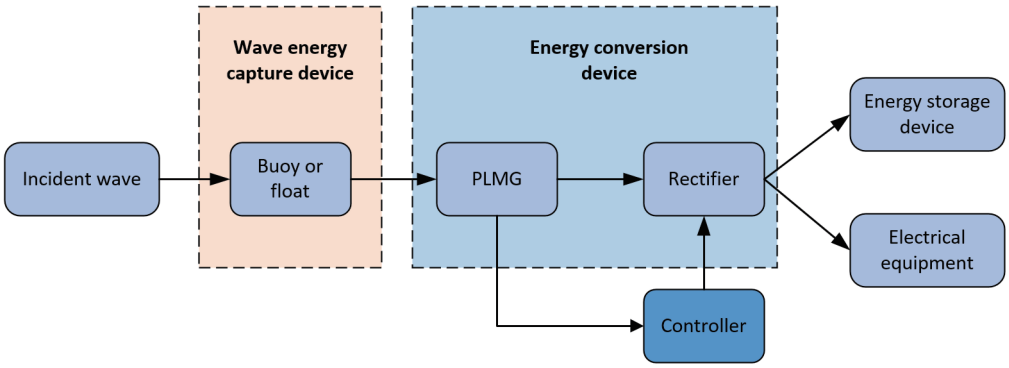

Figure 2. Direct-drive wave energy conversion system workflow chart.

Assumption

(1) No damper winding on the mover and permanent magnet.
(2) The effects of saturation, eddy current, hysteresis, and end effects on motor parameters are ignored.
(3) Permanent magnet magnetomotive force remains constant.
(4) The motor stator's three-phase winding armature resistance and armature inductance are equal.

With the action of the waves, the mover of the linear motor reciprocates up and down in the vertical direction. Therefore, the velocity and frequency of the mover movement are constantly changing. The velocity at which the mover moves upward is defined as the positive direction $v \geq 0$ and downward direction and vice versa.

(i) When $v \geq 0$, stator flux linkage expression is as follows:

$$\psi_s = -Li_{abc} + \psi_{f-abc} \tag{9}$$

where ψ_s is the stator flux vector, $\psi_s = [\psi_a, \psi_b, \psi_c]^T$, i_{abc} is the stator current vector, $i_{abc} = [i_a, i_b, i_c]^T$, L is the inductance matrix and $\psi_{f-\mathrm{abc}}$ is the mover flux linkage of the chain on the stator winding. The matrix representation for L and $\psi_{f-\mathrm{abc}}$ are governed by:

$$L = \begin{bmatrix} L_{ss} & M & M \\ M & L_{ss} & M \\ M & M & L_{ss} \end{bmatrix} \tag{10}$$

$$\psi_{f-\mathrm{abc}} = \begin{bmatrix} \psi_f \sin\frac{2\pi x}{\lambda} \\ \psi_f \sin(\frac{2\pi x}{\lambda} - \frac{2\pi}{3}) \\ \psi_f \sin(\frac{2\pi x}{\lambda} + \frac{2\pi}{3}) \end{bmatrix} \tag{11}$$

where λ is the pole distance of PMLG, ψ_f is the flux linkage on the permanent magnet mover and L_{ss} is the mutual inductance between the stator windings.

The stator voltage equation in *abc*-axis is as follows:

$$u_{s-abc} = -Ri_{abc} + \frac{d(-Li_{abc} + \psi_{f-abc})}{dt} \tag{12}$$

where u_{s-abc} is the stator terminal voltage vector, R is the stator resistance matrix, $R = diag(R_s, R_s, R_s)$ and R_s is the resistance of the stator winding.

Adopting the park transformation of a traditional rotary generator [32], the following transformation to transform the PMLG model in *abc*-axis to the model in *dq*-axis is performed.

As a result, the flux linkage equation becomes

$$\psi_{dq} = D\psi_{f-abc} \tag{13}$$

where D is the transformation matrix expressed as follows:

$$D = \frac{2}{3}\begin{bmatrix} \cos\theta & \cos(\theta - \frac{2\pi}{3}) & \cos(\theta + \frac{2\pi}{3}) \\ -\sin\theta & \sin(\theta - \frac{2\pi}{3}) & -\cos(\theta + \frac{2\pi}{3}) \\ \frac{1}{2} & \frac{1}{2} & \frac{1}{2} \end{bmatrix} \tag{14}$$

where $\theta = \frac{2\pi}{\lambda}x - \frac{\pi}{2}$ is the electrical angle.

When $v \geq 0$, multiplying both sides of the voltage Equation (12) by the transformation matrix D , can be written as follows:

$$u_{dq} = -Ri_{dq} - L_s\frac{di_{dq}}{dt} - L_sAi_{dq} + S\omega\psi_f \tag{15}$$

where A and S are coefficient matrices.

$$A = D\frac{dD^{-1}}{dt} = \omega\begin{bmatrix} 0 & 1 & 0 \\ -1 & 0 & 0 \\ 0 & 0 & 0 \end{bmatrix} \tag{16}$$

$$S = \begin{bmatrix} \cos(2\pi x/\lambda) \\ \cos(2\pi x/\lambda - 2\pi/3) \\ \cos(2\pi x/\lambda + 2\pi/3) \end{bmatrix} = \begin{bmatrix} 0 \\ 1 \\ 0 \end{bmatrix} \tag{17}$$

Substituting A and S into Equation (15), we can obtain

$$u_d = -R_s i_{ds} + \omega L_s i_{qs} - L_s \frac{di_{ds}}{dt} \tag{18}$$

$$u_q = -R_s i_{qs} - \omega L_s i_{ds} - L_s \frac{di_{qs}}{dt} + \omega \psi_f \tag{19}$$

where ω is the angular velocity of PMLG, $\omega = 2\pi v/\lambda$, L_s is the synchronous inductance and $L_s = L_{ss} - M$.

(ii) When $v < 0$, we have

$$\psi_{dq} = -D\psi_{f-abc} \tag{20}$$

Substituting $-u_d$, $-u_q$, $-i_{qs}$, $-i_{ds}$ and ω into (18) and (19), respectively, we have

$$u_d = -R_s i_{ds} - \omega L_s i_{qs} - L_s \frac{di_{ds}}{dt} \tag{21}$$

$$u_q = -R_s i_{qs} + \omega L_s i_{ds} - L_s \frac{di_{qs}}{dt} + \omega \psi_f \tag{22}$$

The anti-electromagnetic force of PMLG equation is expressed as follows:

$$f_g = 3\pi \frac{\psi_f i_q + (L_d - L_q) i_d i_q}{2\lambda} \tag{23}$$

It can be seen from (23) that the anti-electromagnetic force F_g of the PMLG is determined by the stator d-axis and q-axis current components. To reduce losses and improve control efficiency, the zero d-axis vector control strategy is adopted [33], and the magnitude of the anti-electromagnetic force is completely dependent on the magnitude of the stator q-axis current component.

Next, the anti-electromagnetic force of PMLG can be expressed as follows:

$$f_g = \frac{3\pi \psi_f}{2\lambda} i_q \tag{24}$$

Combining with dynamics Equations (7) and (8), the model of DDWEC can be represented by

$$M\ddot{x} = f_e - R_a \dot{x} - kx + \frac{3\pi \psi_f}{2\lambda} i_q \tag{25}$$

3. Controller Design and Stability Analysis

In this section, a BSMC scheme for DDWEC is presented. The control scheme consists of two control steps, namely current control and voltage control. As shown in Figure 3, the rectifier module of the system adopts a three-phase voltage type PWM rectifier, which is composed of the main circuit of the machine side rectifier and the machine side control circuit. The main circuit adopts a three-phase, fully controlled rectifier bridge. The control circuit processes the signals collected from PMLG and provides PWM control signals for the on and off of the switch tube for the three-phase fully controlled rectifier bridge on the machine side. In the controller part, the mover speed tracking d-axis adopts a zero vector control strategy, and the current q-axis adopts BSMC to track the reference current. While in voltage control, a BSMC scheme is utilized to generate the control voltage of SVPWM. In addition, the wave excitation force is in phase with the velocity of the DDWEC.

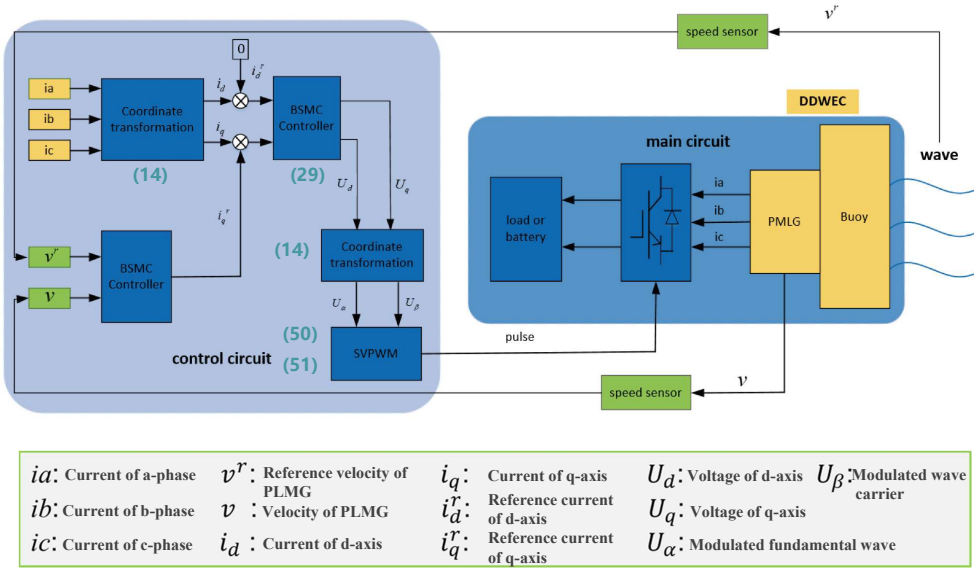

Figure 3. Control block diagram of the overall system.

3.1. Design of i_q^r

Consider the DDWEC model governed by

$$\begin{cases} \dot{x} = v \\ \dot{v} = \frac{1}{M}\left(f_e - R_a\dot{x} - kx + \frac{3\pi\psi_f}{2\lambda}i_q\right) \end{cases} \tag{26}$$

where v is the velocity of PMLG.

Define tracking error as follows:

$$e_1 = x - r \tag{27}$$

where r is the control reference of rotor displacement.

Differentiating (27), we can obtain:

$$\dot{e_1} = v - \dot{r} \tag{28}$$

According to Equations (27), (29) and (32), we can get the control strategy as follows:

$$i_q^r = A(-f_e + R_a\dot{x} + kx - Me_1 - c_1\dot{e_1} - c_2 s + \ddot{r} - \eta\mathrm{sgn}(s)) \tag{29}$$

where $A = 2\lambda/3\pi M\psi_f$, λ is the pole distance of PMLG, ψ_f is the flux linkage on the permanent magnet mover, c_1 and c_2 (positive constants) are the gain of BSMC controller. η (positive constant) is the gain of BSMC controller.

Now, we state the main result of this work.

Theorem 1. *Consider the system (26) under the control law (29), the system is guaranteed to be asymptotically stable and both displacement and velocity errors converge to zero.*

Proof of Theorem 1. Consider a Lyapunov function as follows:

$$V_1 = \frac{1}{2}e_1^2 \tag{30}$$

Differentiating V_1 with respect to time, we have

$$\begin{aligned} \dot{V}_1 &= e_1 \dot{e_1} \\ &= e_1(v - \dot{r}) \end{aligned} \tag{31}$$

Let $v = s - c_1 e_1 + \dot{r}$, where s is the sliding surface, governed by

$$\begin{aligned} s &= v + c_1 e_1 - \dot{r} \\ &= c_1 e_1 + \dot{e_1} \end{aligned} \tag{32}$$

Therefore, it can be concluded:

$$\dot{V}_1 = e_1 s - c_1 {e_1}^2 \tag{33}$$

Consider the following Lyapunov function candidate:

$$V_2 = V_1 + \frac{1}{2} s^2 \tag{34}$$

$$\dot{s} = \frac{1}{M}\left(f_e - R_a \dot{x} - kx + \frac{3\pi\psi_f}{2\lambda} i_q\right) + c_1 \dot{e_1} - \ddot{r} \tag{35}$$

Combining with control law (29), we have

$$\dot{V}_2 = -c_1 e_1^2 - c_2 s^2 - \eta |s| \leq 0 \tag{36}$$

In summary, the proposed BSMC control stategy can make tracking errors $e_1 \to 0$ and $e_2 \to 0$ as $t \to \infty$ which implies that the system is asymptotically stable.

Theorem 1 is proven complete. □

Equations (34) and (36) imply $V_2 > 0$ and $\dot{V}_2 \leq 0$. According to the Lyapunov stability theory and Barbalat's Lemma, the system consisting of V_2 is asymptotically stable. The control and adjustment of displacement x and velocity v are accomplished. Furthermore, the control law i_q^r will be used as a reference current in the sequel.

3.2. Design of PMLG Controller

3.2.1. Forward Motion

When $v \geq 0$, to achieve d-axis and q-axis current tracking, current tracking errors can be simplified as:

$$\begin{cases} e_d = i_d^r - i_d \\ e_q = i_q^r - i_q \end{cases} \tag{37}$$

where i_d and i_q are the d-axis and q-axis current is measured in real time by a sensor in the circuit. i_d^r and i_q^r are reference values for d-axis and q-axis current, $i_d^r = 0$ and i_q^r is governed by (29).

Differentiating (37), we get

$$\begin{aligned} \dot{e}_d =& 0 - \frac{di_d}{dt} \\ =& \frac{1}{L_s}(R_s i_d - \omega L_s i_q + U_d) \end{aligned} \tag{38}$$

$$\begin{aligned} \dot{e}_q =& \dot{i}_q^r - \frac{di_q}{dt} \\ =& A(-f_e + R_a \dot{x} + kx - Me_1 - c_1 \dot{e_1} - c_2 s + \ddot{r} - \eta \mathrm{sgn}(s)) \\ & - \frac{1}{L_s}(R_s i_q + \omega L_s i_d - \omega \varphi_f + U_q) \end{aligned} \tag{39}$$

Then, we can designe the control SVPWM modulation voltage as follows:

$$U_d = -R_s i_d + \omega L_s i_q - c_3 L_s e_d \tag{40}$$

$$\begin{aligned} U_q =& AL_s(-f_e + R_a\dot{x} + kx - Me_1 - c_1\dot{e}_1 - c_2 s + \ddot{r} - \eta \mathrm{sgn}(s)) \\ & - R_s i_q - \omega L_s i_d + \omega \varphi_f + c_4 L_s e_q \end{aligned} \tag{41}$$

where $c_3 > 0$, $c_4 > 0$ are the gain of the proposed controller.

Theorem 2. *Consider the DDWEC model and the current tracking errors under the proposed control strategy (40) and (41). The closed-loop system is guaranteed to be asymptotically stable and both d-axis and q-axis current errors converge to zero.*

Proof of Theorem 2. The following Lyapunov function is selected:

$$V_3 = V_2 + \frac{1}{2}(e_d^2 + e_q^2) \tag{42}$$

Differentiating (42) and after simplification gives

$$\begin{aligned} \dot{V}_3 =& -c_1 e_1^2 - c_2 s - \eta(s) - c_3 e_d^2 + e_d\left(\frac{R_s i_d}{L_s} - \omega i_q + \frac{U_d}{L_s}\right. \\ & \left. + c_3 e_d\right) - c_4 e_q^2 + e_q A(-f_e + R_a\dot{x} + kx - Me_1 \\ & - c_1\dot{e}_1 - c_2 s + \ddot{r} - \eta \mathrm{sgn}(s)) - \frac{e_q}{L_s}(R_s i_q \\ & + \omega L_s i_d - \omega \varphi_f + U_q + c_4 e_q) \end{aligned} \tag{43}$$

Using control law (40) and (41), we have

$$\dot{V}_3 = -c_1 e_1^2 - c_2 s^2 - \eta(s) - c_3 e_d^2 - c_4 e_q^2 \leq 0 \tag{44}$$

In summary, the proposed control strategy (40) and (41) can make the tracking error converge to zero and the entire system is asymptotically stable.

Theorem 2 is proven complete. □

Equations (42) and (44) imply $V_3 > 0$ and $\dot{V}_3 \leq 0$. According to the Lyapunov stability theory and Barbalat's Lemma, the system consisting of V_3 is asymptotically stable. Moreover, the control and adjustment of d-axis current and q-axis current are accomplished. The outputs U_d and U_d will be used as a reference voltage in the sequel.

3.2.2. Reverse Motion

When $v < 0$, the differentiation of d-axis and q-axis current gives

$$\frac{di_d}{dt} = \frac{1}{L_s}(-R_s i_d - \omega L_s i_q - U_d) \tag{45}$$

$$\frac{di_q}{dt} = \frac{1}{L_s}(-R_s i_q + \omega L_s i_d + \omega \varphi_f - U_q) \tag{46}$$

The current tracking errors e_d and e_q are given by

$$\begin{cases} e_d = i_d^* - i_d \\ e_q = i_q^* - i_q \end{cases} \tag{47}$$

where i_d and i_q are the d-axis and q-axis current. i_d^r and i_q^r are reference values for d-axis and q-axis current, $i_d^r = 0$ and i_q^r is governed by (29). Differentiating e_d and e_q, we have

$$\dot{e}_d = \frac{1}{L_s}(R_s i_d + \omega L_s i_q + U_d) \tag{48}$$

$$\begin{aligned}\dot{e}_q =& A(-f_e + R_a\dot{x} + kx - Me_1 - c_1\dot{e}_1 - c_2 s + \ddot{r} - \eta \mathrm{sgn}(s)) \\ & - \frac{1}{L_s}(-R_s i_q + \omega L_s i_d + \omega\varphi_f - U_q)\end{aligned} \tag{49}$$

Then, we can design the control voltage of SVPWM pulse generator as follows:

$$U_d = -R_s i_d - \omega L_s i_q - c_4 L_s e_d \tag{50}$$

$$\begin{aligned}U_q =& AL_s(-f_e + R_a\dot{x} + kx - Me_1 - c_1\dot{e}_1 - c_2 s + \ddot{r} - \eta \mathrm{sgn}(s)) \\ & - R_s i_q - \omega L_s i_d + \omega\varphi_f + c_5 L_s e_q\end{aligned} \tag{51}$$

where $c_4 > 0$, $c_5 > 0$ are the gain of the proposed controller.

Theorem 3. *Consider the system (26) and the tracking errors (47) under the control law (50) and (51). The closed-loop system is guaranteed to be asymptotically stable and both d-axis and q-axis current errors converge to zero.*

Proof of Theorem 3. To ensure the stability of the above subsystems, we construct the following Lyapunov function:

$$V_4 = V_2 + \frac{1}{2}(e_d^2 + e_q^2) \tag{52}$$

Differentiating (52) and after simplification gives

$$\begin{aligned}\dot{V}_4 =& -c_1 e_1^2 - c_2 s - \eta(s) - \mathrm{c}_5 e_d^2 + e_d\left(\frac{R_s i_d}{L_s} + \omega i_q + \frac{U_d}{L_s}\right. \\ & \left. + c_5 e_d\right) - c_6 e_q^2 + e_q A(-f_e + R_a\dot{x} + kx - Me_1 \\ & - c_1\dot{e}_1 - c_2 s + \ddot{r} - \eta \mathrm{sgn}(s)) \\ & + \frac{e_q}{L_s}(R_s i_q - \omega L_s i_d - \omega\varphi_f + U_q + c_6 e_q)\end{aligned} \tag{53}$$

Combining with control laws (50) and (51), we have

$$\dot{V}_4 = -c_1 e_1^2 - c_2 s^2 - \eta(s) - c_5 e_d^2 - c_6 e_q^2 \leq 0 \tag{54}$$

In summary, the proposed control strategy (50) and (51) can make the tracking errors converge to zero and the entire system is asymptotically stable.

Theorem 3 is proven complete. □

Equations (52) and (54) imply $V_4 > 0$ and $\dot{V}_4 \leq 0$. According to the Lyapunov stability theory and Barbalat Lemma, the system consisting of V_4 is asymptotically stable. The control and adjustment of d-axis current and q-axis current are accomplished. Further implementing the output of the reference voltage U_d and U_d.

4. Simulation and Discussion

In this section, to verify the effectiveness of the proposed control algorithm, a simulation model is established on the MATLAB/Simulink based on the BSMC control strategy for DDWEC, whose main parameters are collected in Tables 1 and 2, respectively. The model's parameters are based on the parameters of a typical direct-drive wave energy converter, e.g., the AWS wave energy converter [34]. In this paper, three different parameters for comparative analysis are selected in Table 3 to converge on the sliding mode surface to

ensure the boundedness and stability of the DDWEC system. The simulation results of the comparative analysis are shown in Figure 4. Through the comparison, it can be concluded that parameter 2 has the best tracking performance, specific parameters are as follows: $c_1 = 3$, $c_2 = c_3 = 8$, $c_4 = 10$, $c_5 = c_6 = 15$, and $\eta = 0.1$.

Table 1. Parameters of the DDWEC model.

Parameters	Values	Parameters	Values
m	100 kg	m_a	200 kg
R_a	3500 N	k	2500 N
k_s	6000 N	g	9.8 m/s
ρ	1 g/cm^3	S	0.39 m^3

Table 2. Parameters of the PMLG model.

Parameters	Values	Parameters	Values
L_d	8.2 mH	L_q	8.2 mH
R_s	6.28 Ω	ψ_f	0.147 wb
λ	0.05 m	L_{ss}	3.4 mH

Table 3. Parameters of the BSMC controller.

Parameters	Parameter 1	Parameter 2	Parameter 3
c_1	2	3	5
c_2	6	8	10
c_3	6	8	10
c_4	8	10	15
c_5	8	15	20
c_6	10	15	20
η	0.1	0.1	0.2

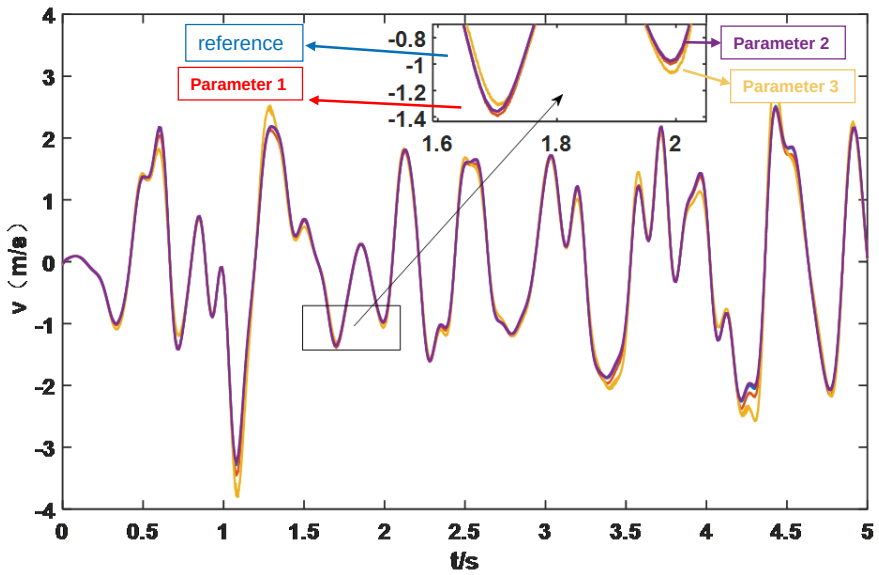

Figure 4. Comparison of the BSMC controller parameters.

Simulation results are shown in Figures 5–11. From Figure 5, the wave data were generated based on the PM spectrum and the phases were completely random. We can see the input wave speed; irregular waves can better reflect the performance of the control system. From Figure 6, we can see the error of the velocity under the improved BSMC method, which can track the reference velocity and displacement with a faster speed and more precisely compared with the PIR strategy. The PIR strategy has obvious instability

in the whole tracking process, but the BSMC strategy we designed can perfectly solve this problem and ensure reliable tracking accuracy. Reference and actual states of i_d and i_q are shown in figure Figures 7 and 8, zero vector control strategy is adopted for the d-axis. The essence of controlling the translator speed is to change the current of the q-axis, then change the conduction sequence of the rectifier switch and change the equivalent damping of the system, from which we can see the current under the BSMC method can track the reference current more precisely. Figure 9 shows the *abc* three-phase current, *abc* three-phase current is obtained by inverse transformation of the dq-axis and the reason for the irregularity of the current is due to the tracking of changing wave movements. From Figure 10, it can be seen that the BSMC method is a more suitable technology than the other method for DDWEC applications since more energy and smaller fluctuations can be achieved. The peak power of DDWEC in a single wave period changes according to the change of wave displacement, and the maximum peak is 1500W. In summary, simulation and comparison results demonstrate that the proposed EMPC-FTSMC scheme can achieve exact wave energy tracking and disturbance rejection simultaneously.

The actual capture energy and the expected performance of capture energy of the BSMC algorithm in five seconds are shown in the Figure 11. The actual captured energy within five seconds of the BSMC algorithm is 96% of the optimal captured energy, and the simulation results show that the designed controller has great performance and considerable wave energy capture efficiency. The control strategy we designed in this paper has a high practical application prospect.

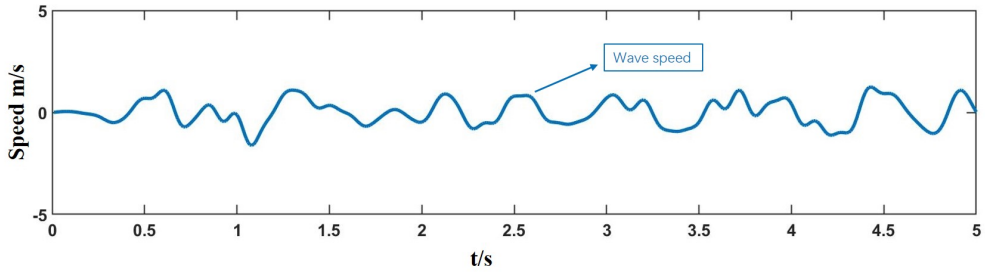

Figure 5. Input of wave velocity.

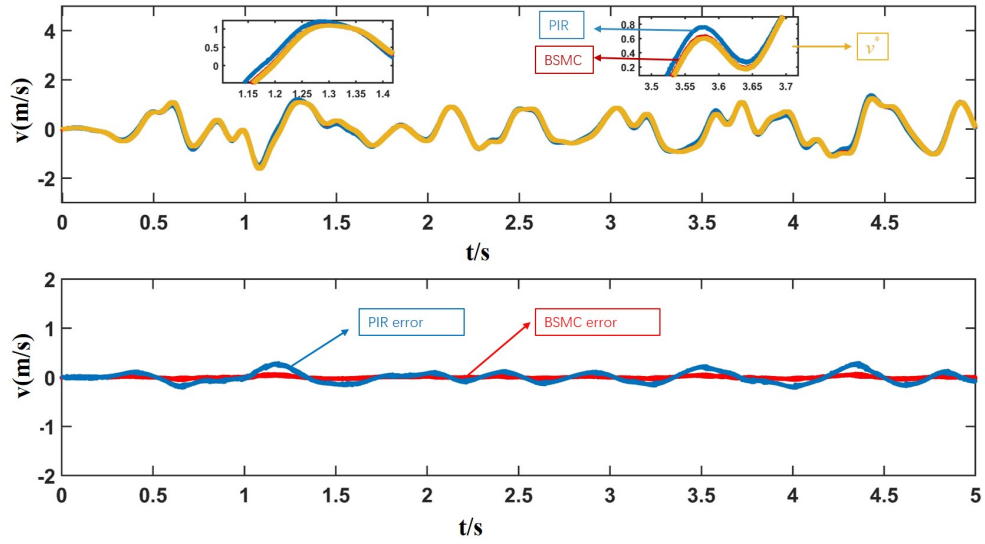

Figure 6. Desired and actual states and tracking error for v.

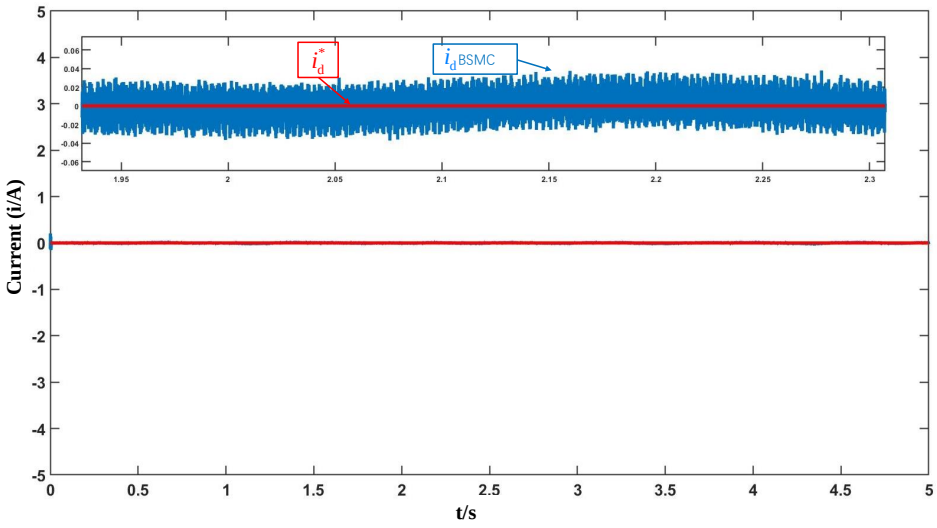

Figure 7. Current of *d*-axis.

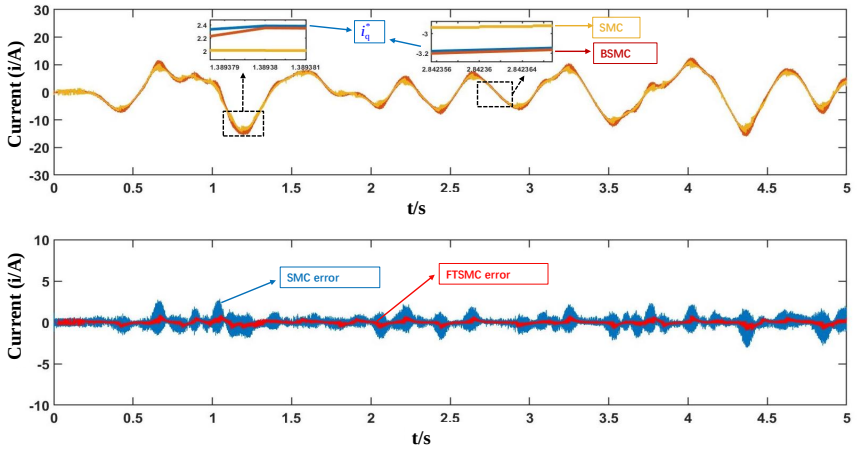

Figure 8. Current of *q*-axis.

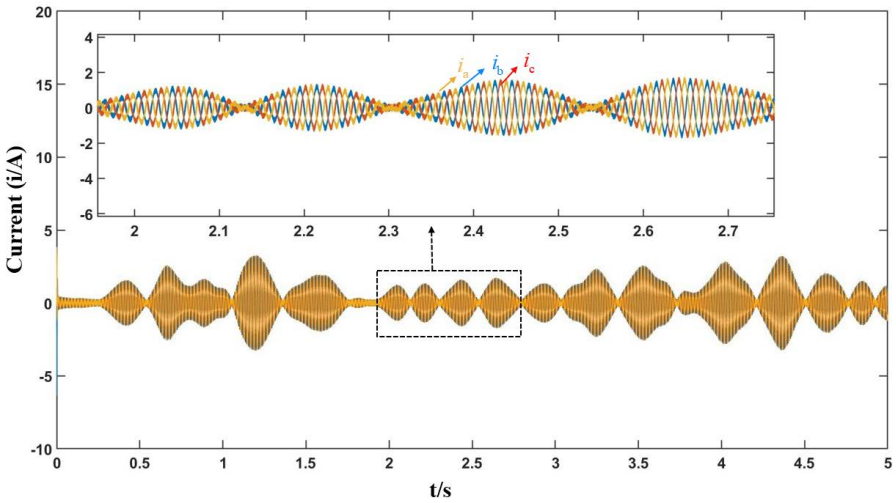

Figure 9. Current of *abc*-axis.

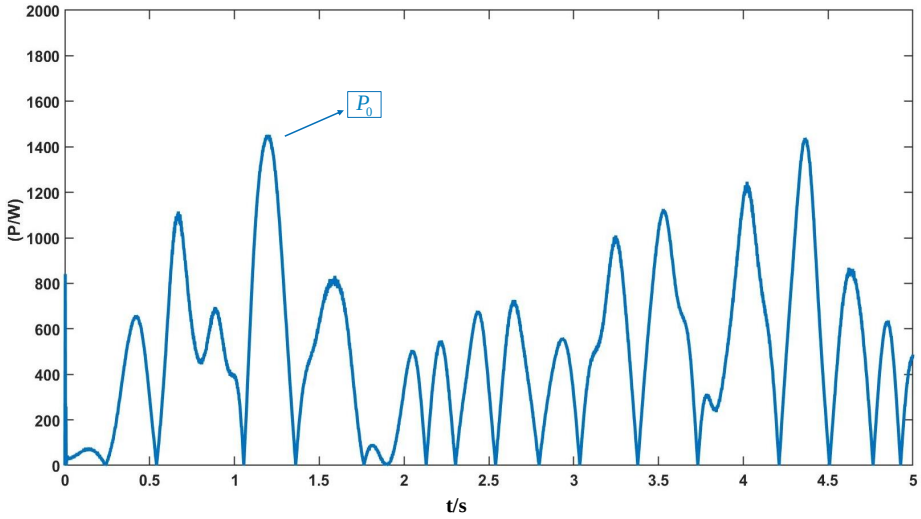

Figure 10. Power control simulation of DDWEC.

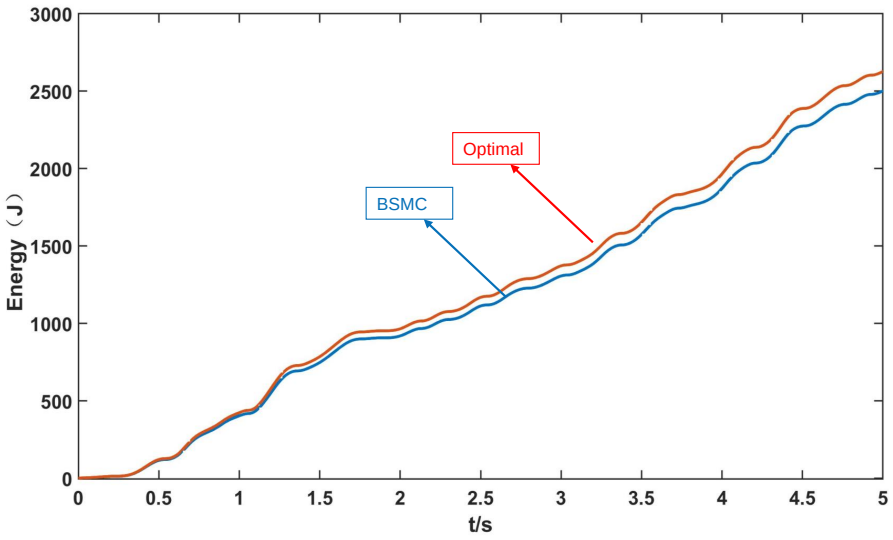

Figure 11. Actual capture energy and optimal capture energy.

5. Conclusions

In this paper, the BSMC scheme was proposed to enhance the energy tracking capability of DDWEC. By using the method of directly tracking the velocity of the incident wave, the wave energy can be more precisely tracked. The vertical velocity of the wave was tracked by the proposed BSMC and the velocity information was fed back to the linear generator in real-time. A novel controller has been designed to adjust the velocity of the linear generator online. Finally, the DDWEC system based on the BSMC scheme reached resonance and completed high-performance energy tracking of waves. The maximum power peak value is 1500 W. At this time, the motor mover follows the wave to reach the peak value of 1.91 m/s. Due to the wave fluctuation, the motion of the linear motor mover is irregular. The wave resonates with the linear motor mover, and the system outputs the maximum power. The simulation results show that the captured energy of the BSMC control method is 3.8% higher than that of SMC. In future works, wave dynamics can be considered and the energy tracking of DDWEC is expected to be achieved in real-life.

Author Contributions: Methodology, S.W.; software, S.W.; validation, S.W.; formal analysis, J.W.; resources, J.W.; data curation, J.W.; writing—original draft preparation, S.W.; writing—review and editing, S.W. All authors have read and agreed to the published version of the manuscript.

Funding: This research received no external funding.

Institutional Review Board Statement: Not applicable.

Informed Consent Statement: Not applicable.

Data Availability Statement: The partial data can be found in this paper.

Conflicts of Interest: The authors declare no conflict of interest.

References

1. Liu, C.; Zhu, H.; Dong, R. Sensitivity analysis and Optimal design of a linear magnetic gear for direct-drive wave energy conversion. *IEEE Access.* **2019**, *7*, 73983–73992. [CrossRef]
2. Wilkinson, L.; Whittaker, T.J.T.; Thies, P.R. The power-capture of a nearshore, modular, flap-type wave energy converter in regular waves. *Ocean Eng.* **2017**, *137*, 394–403. [CrossRef]
3. Ringwood, J.V.; Bacelli, G.; Fusco, F. Energy-maximizing control of wave-energy converters: The development of control system technology to optimize their operation. *IEEE Trans. Syst. Mag.* **2014**, *34*, 30–55.
4. Antonio, F.O. Wave energy utilization: A review of the technologies. *Renew. Sust. Energ. Rev.* **2010**, *14*, 899–918.
5. Mendonca, H.; Martinez, S. A resistance emulation approach to optimize the wave energy harvesting for a direct drive point absorber. *IEEE Trans. Sustain. Energy* **2015**, *7*, 3–11. [CrossRef]
6. Babarit, A.; Clément, A.H. Optimal latching control of a wave energy device in regular and irregular waves. *Appl. Ocean Res.* **2006**, *28*, 77–91. [CrossRef]
7. Tedeschi, E.; Molinas, M. Impact of control strategies on the rating of electric power take off for wave energy conversion. In Proceedings of the 2010 IEEE International Symposium on Industrial Electronics, Bari, Italy, 4–7 July 2010; pp. 2406–2411.
8. Shek, J.K.H.; Macpherson, D.E.; Mueller, M.A. Reaction force control of a linear electrical generator for direct drive wave energy conversion. *IET Renew.* **2007**, *1*, 17–24. [CrossRef]
9. Bacelli, G.; Coe, R.G. Comments on control of wave energy converters. *IEEE Trans. Contr. Syst. Technol.* **2020**, *29*, 478–481. [CrossRef]
10. Marei, M.I.; Mokhtar, M.; El-Sattar, A.A. MPPT strategy based on speed control for AWS-based wave energy conversion system. *Renew. Energy* **2015**, *83*, 305–317. [CrossRef]
11. Lopes, M.F.P.; Hals, J.; Gomes, R.P.F. Experimental and numerical investigation of non-predictive phase-control strategies for a point-absorbing wave energy converter. *Ocean Eng.* **2009**, *36*, 386–402. [CrossRef]
12. Neshat, M.; Sergiienko, N.Y.; Mirjalili, S.; Majidi Nezhad, M.; Piras, G.; Astiaso Garcia, D. Multi-mode wave energy converter design optimisation using an improved moth flame optimisation algorithm. *Energies* **2021**, *14*, 3737. [CrossRef]
13. Ciappi, L.; Simonetti, I.; Bianchini, A.; Cappietti, L.; Manfrida, G. Application of integrated wave-to-wire modelling for the preliminary design of oscillating water column systems for installations in moderate wave climates. *Renew. Energy* **2022**, *194*, 232–248. [CrossRef]
14. Ciappi, L.; Cheli, L.; Simonetti, I.; Bianchini, A.; Manfrida, G.; Cappietti, L. Wave-to-wire model of an oscillating-water-column wave energy converter and its application to mediterranean energy hot-spots. *Energies* **2020**, *13*, 5582. [CrossRef]
15. Henriques, J.; Portillo, J.; Sheng, W.; Gato, L.; Falcão, A. Dynamics and control of air turbines in oscillating-water-column wave energy converters: Analyses and case study. *Renew. Sustain. Energy Rev.* **2019**, *112*, 571–589. [CrossRef]
16. Henriques, J.; Gato, L.; Lemos, J.; Gomes, R.; Falcão, A. Peak-power control of a grid-integrated oscillating water column wave energy converter. *Energy* **2016**, *109*, 378–390. [CrossRef]
17. Eltamaly, A.M.; Farh, H.M. Dynamic global maximum power point tracking of the PV systems under variant partial shading using hybrid GWO-FLC. *Sol. Energy* **2019**, *177*, 306–316. [CrossRef]
18. Sangwongwanich, A.; Blaabjerg, F. Mitigation of interharmonics in PV systems with maximum power point tracking modification. *IEEE Trans. Power Electron.* **2019**, *34*, 8279–8282. [CrossRef]
19. Napole, C.; Derbeli, M.; Barambones, O. Fuzzy logic approach for maximum power point tracking implemented in a real time photovoltaic system. *Appl. Sci.* **2021**, *11*, 5927. [CrossRef]
20. Mirza, A.F.; Mansoor, M.; Zhan,K.; Ling, Q. High-efficiency swarm intelligent maximum power point tracking control techniques for varying temperature and irradiance. *Energy* **2021**, *228*, 120602. [CrossRef]
21. Pan, L.; Zhu, Z.; Xiong, Y.; Shao, J. Integral sliding mode control for maximum power point tracking in DFIG based floating offshore wind turbine and power to gas. *Processes* **2021**, *9*, 1016. [CrossRef]
22. Elsonbaty, N.A.; Enany, M.A.; Elymany, M. Proposed rotor field-oriented maximum power point tracking polices for permanent magnet synchronous generator-based wind turbine. *Wind Eng.* **2021**, *45*, 973–991. [CrossRef]
23. Amon, E.A.; Brekken, T.K.; Schacher, A.A. Maximum power point tracking for ocean wave energy conversion. *IEEE Trans. Ind. Appl.* **2012**, *48*, 1079–1086. [CrossRef]

24. António, F.D.O. Modelling and control of oscillating-body wave energy converters with hydraulic power take-off and gas accumulator. *Ocean Eng.* **2007**, *34*, 2021–2032.
25. Kavya, M.; Jayalalitha, S. A novel coarse and fine control algorithm to improve Maximum Power Point Tracking (MPPT) efficiency in photovoltaic system. *ISA Trans.* **2022**, *121*, 180–190.
26. Nguyen, A.T.; Rafaq, M.S.; Choi, H.H.; Jung, J.W. A model reference adaptive control based speed controller for a surface-mounted permanent magnet synchronous motor drive. *IEEE Trans. Ind. Electron.* **2018**, *65*, 9399–9409. [CrossRef]
27. Zhao, A.; Wu, W.; Sun, Z.; Zhu, L.; Lu, K.; Chung, H.; Blaabjerg, F. A flower pollination method based global maximum power point tracking strategy for point-absorbing type wave energy converters. *Energies* **2019**, *12*, 1343. [CrossRef]
28. Zhan, S.; Li, G.; Na, J.; He, W. Feedback noncausal model predictive control of wave energy converters. *Control Eng. Pract.* **2019**, *85*, 110–120. [CrossRef]
29. Zhan, S.; Li, G.; Bailey, C. Economic feedback model predictive control of wave energy converters. *IEEE Trans. Ind. Electron.* **2019**, *67*, 3932–3943. [CrossRef]
30. Tom, N.; Yeung, R.W. Experimental confirmation of nonlinear-model-predictive control applied offline to a permanent magnet linear generator for ocean-wave energy conversion. *IEEE J. Ocean. Eng.* **2015**, *41*, 281–295.
31. de la Villa-Jaen, A.; El Montoya-Andrade, D.; Garcia-Santana, A. Control strategies for point absorbers considering linear generator copper losses and maximum excursion constraints. *IEEE Trans. Sus. Energy* **2018**, *9*, 433–442. [CrossRef]
32. Pillay, P.; Krishnan, R. Modeling, simulation, and analysis of permanent-magnet motor drives. I. The permanent-magnet synchronous motor drive. *IEEE Trans. Ind. Appl.* **1989**, *25*, 265–273. [CrossRef]
33. Chinchilla, M.; Arnaltes, S.; Burgos, J.C. Control of permanent-magnet generators applied to variable-speed wind-energy systems connected to the grid. *IEEE Trans. Energy Convers.* **2006**, *21*, 265–273. [CrossRef]
34. Polinder, H.; Damen, M.E.C.; Gardner, F.Linear PM generator system for wave energy conversion in the AWS. *IEEE Trans. Energy Convers.* **2004**, *19*, 583–589. [CrossRef]